Journal of Bio- and Tribo-Corrosion (2020) 6:34
https://doi.org/10.1007/s40735-020-0329-2

New Synthesized Nicotinonitrile Derivatives as Effective Corrosion Inhibitors for Carbon Steel in Acidic Environment: Electrochemical, Surface Analysis, and Quantum Methods

A. S. Fouda[1] · A. H. El-Askalany[1] · A. F. Melouk[1] · N. S. Elsheikh[1]

Received: 18 September 2019 / Revised: 10 January 2020 / Accepted: 29 January 2020 / Published online: 10 February 2020

Abstract
2-((2-Aminophenyl)thio)-4,6-dimethylnicotinonitrile (APTDN) and 4,6-dimethyl-2-(phenylamino) nicotinonitrile (DPAN) as new organic derivatives were investigated as corrosion inhibitors for C-steel in 1 M HCl at various temperatures (25–45 °C) using chemical and electrochemical methods. The adsorption of inhibitors on the C-steel surface fits to Langmuir adsorption isotherm and polarization curves showed that APTDN and DPAN are mixed corrosion inhibitors. The topography maps of atomic force microscopy, X-ray photoelectron spectroscopy, and Attenuated total refraction infrared were performed for examination of C-steel surface. Moreover, quantum chemical calculations using Density functional theory were carried out to correlate between theoretical and experimental data.

Keywords C-steel · HCl · Corrosion inhibition · ATR-IR · XPS · AFM

1 Introduction

Metallic corrosion is a material problem that began from the discovery of metal [1]. Corrosion refers to any change that occurs in the features of metals and alloys due to physico-chemical interaction with its surrounding environments and this has resulted in weakness of the role of the metal, the surrounding, or the technical system of which these form a part [2]. C-steel is the engineering material in many industrial applications like pipes, pumps, turbine blades, and water coolers and heaters [3]. Surface of these equipments is being destroyed as result of the formation of less reactive oxides that accumulate in the process of rust and scales; hence, the life time of these materials is cut short as a result of corrosion [4]. Concentrated acidic medium such as hydrochloric acid is used to remove these produces by pickling, degreasing, and descaling processes [5, 6]. Thus, during this chemical treatment, adding corrosion inhibitors is significant to decrease the corrosive impact; particularly, the usage of organic inhibitors is effective due to their activity at a variety of temperatures, good solubility, and comparatively low toxicity [7, 8].

However, organic substances especially heterocyclic compounds constitute inhibitive boundary at the metallic/atmosphere interfaces through adsorption process. These have an important role by transmitting their unshared electron pair into the d-vacant orbit of the metal ion to form coordinate bond via chemical adsorption [9] or physical adsorption involving electrostatic interaction.

The interest in nicotinonitrile derivatives is due to the practical use as medicinal compounds and the existence of the pyridine ring that play an important place in organic synthesis. The literature review of some studies reveal that some nicotinonitrile derivatives have been reported as effective inhibitors for steel corrosion [10, 11]. Several authors before have used organic derivatives as corrosion inhibitors for steel in acid medium [12–21]. Here, we investigate new organic inhibitors, namely, 2-((2-aminophenyl) thio)-4,6-dimethylnicotinonitrile(APTDN) and 4,6-dimethyl-2-(phenylamino) nicotinonitrile (DPAN), which were considered an effective corrosion inhibitor for C-steel in 1 M hydrochloric acid. The inhibitory effect was investigated using mass loss, potentiodynamic polarization (PP), electrochemical impedance spectroscopy (EIS), electrochemical frequency modulation (EFM), surface

✉ A. S. Fouda
asfouda@hotmail.com

[1] Chemistry Department, Faculty of Science, Mansoura University, Mansoura 35516, Egypt

characterization by AFM and XPS, and quantum chemical calculations.

The present research explores the inhibition effect of the two synthesized nicotinonitrile derivatives, namely, 2-((2-aminophenyl) thio)-4, 6-dimethylnicotinonitrile (APTDN) and 4,6-dimethyl-2-(phenylamino) nicotinonitrile (DPAN) on the corrosion of C-steel in 1 M HCl.

2 Experimental Methods

2.1 Metallic Materials

The present C-steel samples used for experimental methods have the following chemical composition (weight %): Si 0.25%, C 0.2%, Mn 0.5%, S 0.05%, and Fe 99%. For mass loss method, the samples were mechanically cut into $2.0\times2.0\times0.2$ cm dimensions then hand polished by emery papers with varied grades from 400 upto 2000 grit size until the surface became like a mirror, degreased with acetone to remove impurities, washed by twice distilled water, and finally dried with filter papers. The working electrode used in PP, EIS, and EFM techniques has an exposed area of 1 cm^2 (the edges of the samples were covered with the epoxy resin) and was abraded and degreased like the prior method.

2.2 Synthesis of the Inhibitors

Nicotinonitrile derivatives were synthesized by many steps starting from preparation of 3-cyano-4,6-dimethylpyridine-2-one **1** according to the reported method of Bardhan [12] by stirring acetylacetone with cyanoacetamide in ethyl alcohol and potassium carbonate (Scheme 1). Heating of this pyridine **1** with phosphorus oxychloride furnished 2-chloro-4,6-dimethylnicotinonitrile **2** [22, 23] which has been utilized as a precursor for the synthesis of 2-(2-aminophenylthio)-4,6-dimethylnicotinonitrile **3** through its heating with *o*-aminothiophenol in ethanol and potassium carbonate [24]. Furthermore, the chlorine atom of 2-chloronicotinonitrile derivative 4 proved to be reactive towards nucleophilic substitution by nitrogen nucleophile such as aniline to afford 2-anilino-4,6-dimethylnicotinonitrile **4**.

2.3 Solutions

The corrosive solution (1 M HCl, analytical reagent grade 37%) was prepared by using twice distilled water. Inhibitor's stock solutions (10^{-3} M) were prepared by dissolving (APTDN) and (DPAN) in ethanol then mitigated by using twice distilled water to get the concentration range $(2–10)\times10^{-5}$ M). The quantity of ethanol was kept constant in each preparation to get rid the impact of ethanol on the inhibition efficiency.

2.4 Mass Loss (ML) Measurements

The mass loss method is the high accuracy method for laboratory corrosion study as well to calculate the corrosion rate (C.R.) and inhibition efficiency (η). The previously prepared specimens of the metal were massed and dipped in the corrosive media in the absence and presence of studied additives (APTDN and DPAN) at varied concentrations for a certain time of 3 h. Every half hour, the sample is taken out, washed,

Scheme 1 .

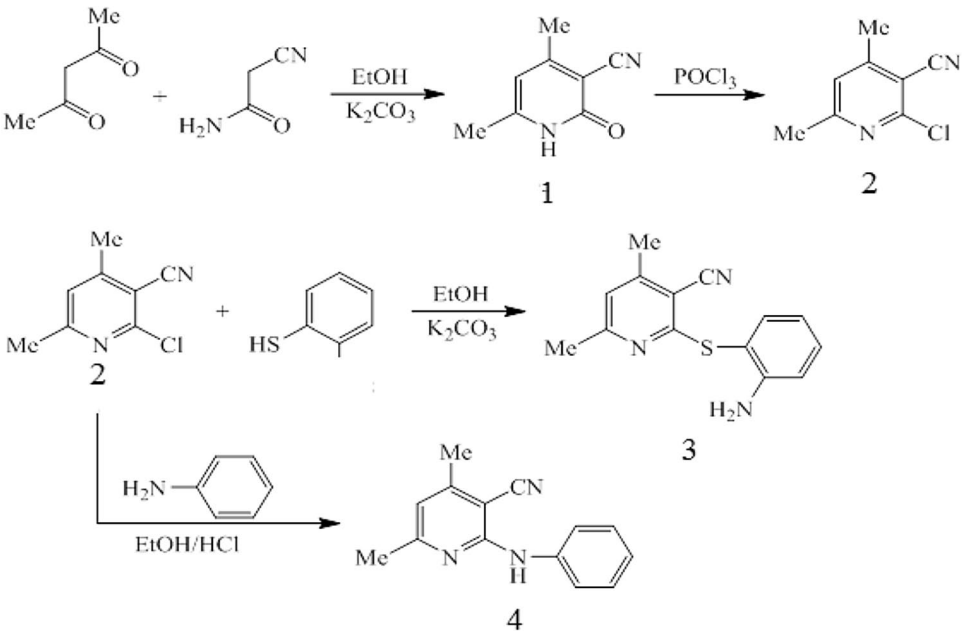

dried and finally weighed accurately. The mean mass loss (ΔW) was calculated using Eq. (1) [25]

$$\Delta W = W_1 - W_2, \tag{1}$$

where W_1 *and* W_2 are the mass losses of specimens prior and after dipping in the test solution.

The inhibitor efficiency ($\eta\%$) and the degree of surface coverage (θ) in the presence of the studied additives (APTDN and DPAN) were calculated using Eq. (2)

$$\eta\% = \theta \times 100 = \left[1 - \frac{W_{\text{inh}}}{W_{\text{free}}}\right] \times 100, \tag{2}$$

where W_{inh} and W_{free} are the mean mass losses in the presence and absence of inhibitors, respectively.

2.5 Electrochemical Measurements

The electrochemical method is the most powerful method to give information about metal–inhibitor interaction as a result of the metallic corrosion which involves anodic and cathodic reactions. Electrochemical tests were performed at a three-electrode cell configuration: the working electrode (Carbon Steel electrode), the reference electrode (saturated calomel electrode placed in a fine capillary), and the counter electrode (Pt wire). These tests involve three parts: impedance spectroscopy, potentiodynamic polarization, and electrochemical frequency modulation tests, respectively. The working electrode was dipped in the test medium for 30 min until the (steady state potential) open circuit potential OCP is reached which is determined as the tendency of a metallic surface to be corroded freely in any corrosive medium [26].

Potentiodynamic polarization tests were applied at OCP by varying the electrode potential from − 500 to 500 mV with a scan rate of 1 mV/s. EIS test used AC signals at OCP with frequency range starting from 0.01 Hz at low frequency to 100,000 Hz at high frequency with applied potential signal amplitude of + 10 mV around the rest potential. Lastly, EFM test was made with small potential perturbation signal and amplitude 10 mV with two sine waves of 2 and 5 Hz.

2.6 ATR-IR Spectroscopy Analysis

The chemical composition of APTDN and DPAN was studied by ATR-IR (Thermo Fisher Scientific, NicoletiS10 model) analysis. Infrared spectra were recorded using ATR (Attenuated Total Reflection) in the wavenumber range 400–4000 cm^{-1}.

2.7 Atomic Force Microscopy (AFM) Analysis

The surfaces of C-steel samples were observed in non-contact mode atomic force microscopy (Pico SPM2100) and before analysis the specimens were abraded by emery papers upto 2000 grit size until reaching uniform surface and then immersed in the aggressive solution for 24 h without and with APTDN and DPAN at 25^{O}C. Then the specimens were removed from the solution, washed well, dried, and analyzed in AFM instrument.

2.8 Quantum Chemical Study

The correlation between the molecular structure of investigated compounds and their quantum chemical parameters was examined using Materials Studio version 7.0.

2.9 X-Ray Photoelectron Spectroscopy Analysis

The surface of carbon steel after its immersion in 1 M HCl solution in the absence and presence of 10^{-4} M APTDN and DPAN for 24 h was characterized by XPS K-ALPHA (Themo Fisher Scientific, USA) using monochromatic X-ray Al K-alpha radiation of -10 to 1350 eV and spot size of 400 micro m at a pressure range of 10–9 mbar with full spectrum pass energy of 200 eV and narrow spectrum pass energy of 50 eV.

3 Results and Discussion

3.1 Mass Loss (ML) Measurements

3.1.1 Effect of Inhibitor Concentration

Figure 1 shows the ML–time curves for C-steel in 1 M HCl in the absence and presence of various concentrations of APTDN with range (2×10^{-5} to 1×10^{-4}) M at 25 ± 0.1 °C. Other curves were obtained for DPNA (not shown). The existence of a linear relation between the ML and time is clear from the figure. This behavior shows the adsorption of additives on C-steel surface and impedes the corrosion process [27]. Corrosion parameters such as corrosion rate (C.R.), degree of surface coverage (θ), and inhibition efficiency %η for APTDN and DPAN compounds are recorded in Table 1. The data illustrate that an increase in the concentration of the two inhibitors leads to a decrease in the C.R. and an increase the η%. Obviously, compound APTDN shows higher values of %η than DPAN.

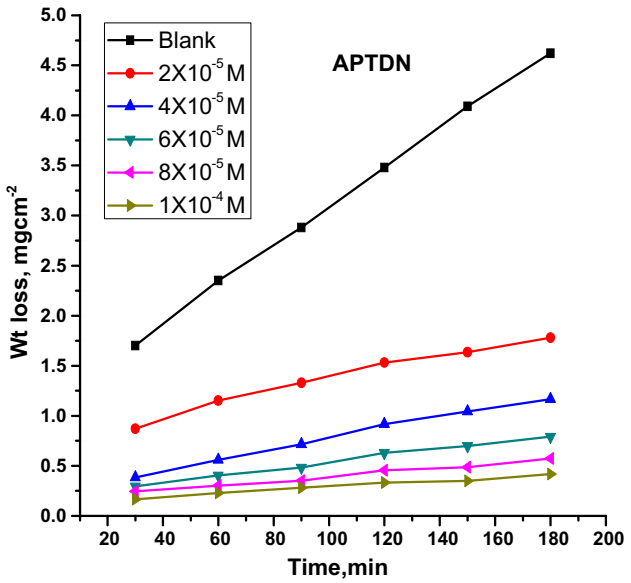

Fig. 1 ML versus time plot for the dissolution of C-steel with and without different concentrations of APTDN in 1 M HCl at 25 °C

Table 1 Data of ML method for corrosion of C-steel in 1 M HCl solution with and without different concentrations of APTDN and DPAN additives at 25 °C

Inhibitors	Conc. M	C.R. (mg/cm^2/min)	θ	$\%\eta$
1 M HCl	Blank	0.029	–	–
APTDN	2×10^{-5}	0.013	0.560	56.0
	4×10^{-5}	0.008	0.736	73.6
	6×10^{-5}	0.005	0.834	83.4
	8×10^{-5}	0.004	0.869	86.9
	1×10^{-4}	0.003	0.905	90.5
DPAN	2×10^{-5}	0.014	0.523	52.3
	4×10^{-5}	0.012	0.575	57.5
	6×10^{-5}	0.011	0.612	61.2
	8×10^{-5}	0.009	0.707	70.7
	1×10^{-4}	0.005	0.819	81.9

3.1.2 Effect of Temperature

To study the effect of investigated compounds at higher temperatures, ML measurements were performed at different temperatures (25–45 °C). The variation of $\%\eta$ with the solution temperatures are shown in Fig. 2 which indicated that the $\%\eta$ increased with an increase in temperature. At all studied temperatures, the order of $\%\eta$ was in the order: APTDN > DPAN. The little increase or constancy in the $\%\eta$ with increases of temperature is related to the chemical adsorption only or due to the combination of physical and chemical adsorption [28].

3.1.3 Adsorption Isotherms

The adsorption isotherm is a powerful tool to study the adsorption behavior of the investigated compounds on metallic surface. Various isotherms including Frumkin, Langmuir, Temkin, and Freundlich were studied to fit the experimental results by plotting the calculated degree of surface coverage (θ) against different concentrations of APTDN and DPAN additives as shown in Fig. 3. Straight lines in both additives with the correlation coefficient R^2 approach unity, indicating that the Langmuir adsorption isotherm is the best linear fit to the results. The equilibrium constant K_{ads} is given from Eq. (3) [29] by using the relation between C and C/θ

$$\frac{C}{\theta} = \left(\frac{1}{K_{ads}}\right) + C \tag{3}$$

The values of K_{ads} were used to calculate the value of adsorption of Gibbs free energy ΔG^{o}_{ads} through Eq. (4) [30]:

$$K_{ads} = \frac{1}{55.5}\exp\left(\frac{-\Delta G^{o}_{ads}}{RT}\right) \tag{4}$$

The value of 55.5 refers to the molar concentration of H_2O_{sol} in aqueous solution (in M/L).

The negative values (Table 2) of the calculated ΔG^{o}_{ads} indicate the spontaneity of the substitution adsorption process between H_2O_{ads} and organic molecule org_{aq} at the interface [31]

$$Org_{(sol)} + x\left(H_2O\right)_{ads} \leftrightarrow Org_{(ads)} + xH_2O_{(sol)}$$

Moreover, the ΔG^{o}_{ads} values reached − 47 kJ mol^{-1} which reflects a high chemical adsorption on the steel surface. In general, the ΔG^{o}_{ads} values of − 40 kJ mol^{-1} or more are attributed to chemisorption through the charge transfer between the inhibitor molecule and the metal surface to form coordinate bond [32]. Additionally, the observed value of ΔG^{o}_{ads} − 36.8 kJ mol^{-1} is related to physisorption via electrostatic interaction. Thus, it is established that the type of the adsorption for APTDN and DPAN molecules is a mixed type i.e. chemical and physical adsorption with mainly chemical [31]. As well, the enthalpy (ΔH^{o}_{ads}) and the entropy (ΔS^{o}_{ads}) of adsorption are calculated by the Van't Hoff [33] and thermodynamic equations (Eqs. 5, 6), respectively:

$$\ln K_{ads} = \frac{-\Delta H^{o}}{RT} + \text{constant}, \tag{5}$$

$$\Delta G^{o}_{ads} = \Delta H^{o}_{ads} - T\Delta S^{o}_{ads} \tag{6}$$

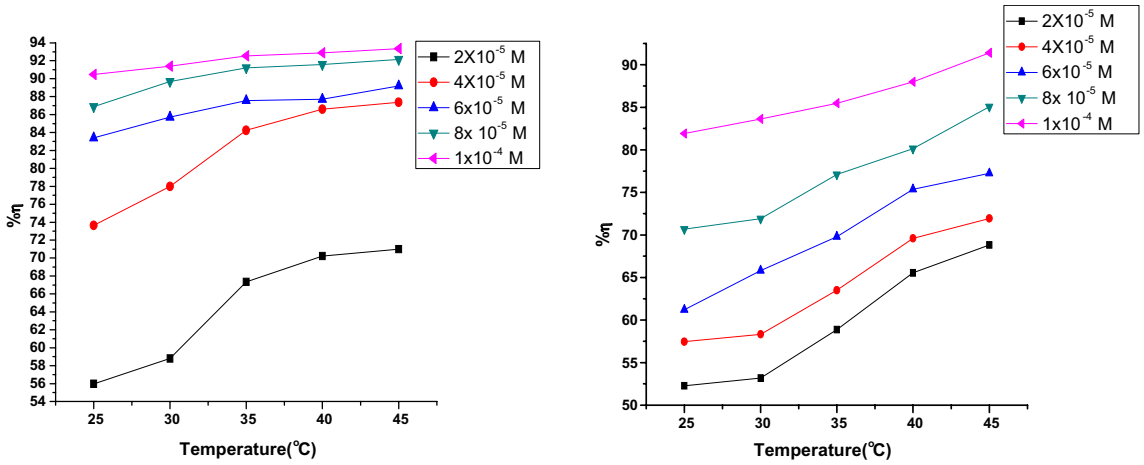

Fig. 2 Difference of %η against temperatures for additives APTDN and DPAN

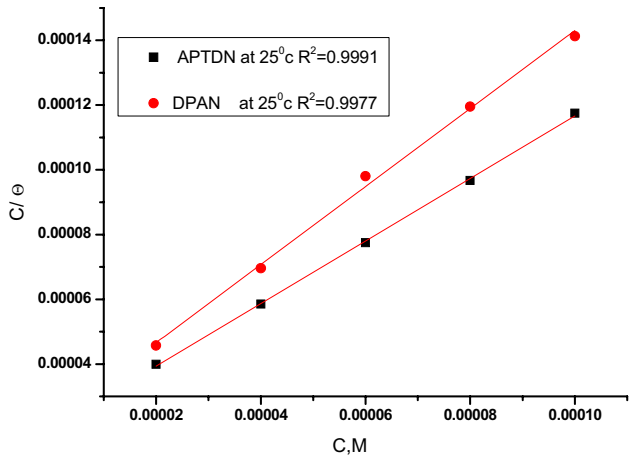

Fig. 3 Langmuir isotherm drawn as [C/θ] versus [C] of APTDN and DPAN molecules for corrosion of C-steel in 1 M HCl at 25 °C

Table 2 Thermodynamic adsorption parameters of APTDN and DPAN adsorbed on C-steel surface in 1 M HCl at various temperatures

Inhibitor	Temp °C	$K_{ads} \times 10^{-3}$ M^{-1}	$-\Delta G^{\circ}_{ads}$ kJ/mol	ΔH°_{ads} kJ/mol	ΔS°_{ads} J/mol K
APTDN	25	50.1	36.8	13.3	123.4
	30	77.6	38.5		127.1
	35	108.5	40.0		129.8
	40	282.2	43.1		137.8
	45	995.6	47.1		148.3
DPAN	25	44.4	36.5	10.6	122.4
	30	61.8	38.0		160.1
	35	107.6	40.0		164.1
	40	121.8	41.0		164.6
	45	451.0	45.0		174.9

The calculated enthalpy (ΔH^{o}_{ads}) values in both the studied additives have a positive sign, indicating the endothermic nature of the adsorption process. This confirms that the chemisorption is taking place on the steel surface. Finally, the standard adsorption entropy ΔS^{o}_{ads} is increased in positive direction indicating that the adsorbed layer formed on the steel surface of the two additives is due to the desorption of a high number of water molecules [H_2O_{ads}] from surface by APTDN and DPAN molecules in the aqueous solution [APTDN (sol), DPAN (sol)] [34].

3.1.4 Thermodynamic Activation Parameters

The mechanistic information about the adsorption process of the inhibitor molecule on the surface of metallic material is determined by the value of activation energy. To calculate the value of activation energy, the logarithm of the C.R. (mg/cm^2/min) is plotted versus 1/T for 1 M HCl with and without various molar concentrations of APTDN, according to the Arrhenius equation:

$$\log \text{C.R.} = \left[-E^{*}_{a}/2.303RT\right] + \log A, \tag{7}$$

where (A) is the frequency factor, (E_a^*) is the apparent activation energy, R is the gas constant, and (T) is the absolute temperature. Figure 4 shows straight lines with a slope equal to ($-E_a^*/2.303R$) at which activation parameters can be obtained. Table.3 shows the relatively higher value of the activation energy, E_a^*, in the blank solution when compared to E_a^* in the presence of the two studied additives (APTDN and DPAN); this is attributed to its chemical adsorption on the C-steel surface, whereas the opposite is right for physical adsorption [35].

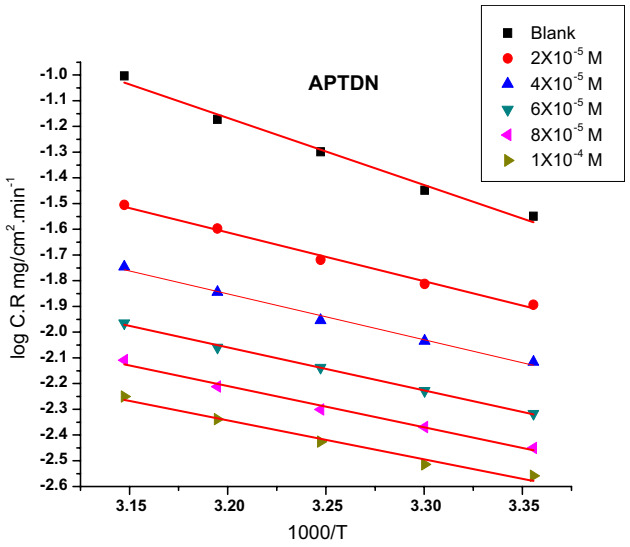

Fig. 4 Arrhenius plots (log C.R. vs 1000/*T*) for C-steel in 1 M HCl with and without various concentrations of APTDN

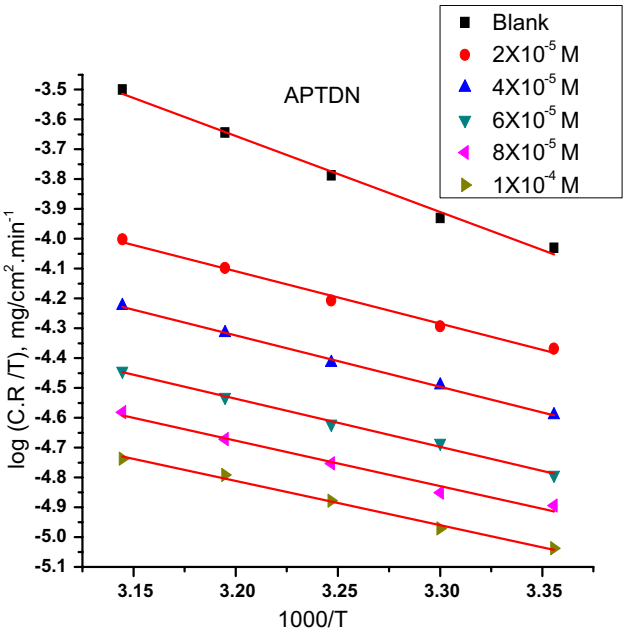

Fig. 5 The Transition state plot (log C.R./*T* vs 1000/*T*) for C-steel in 1 M HCl in the absence and presence of different concentrations of APTDN

Table 3 Activation parameters for the corrosion of C-steel in absence and presence of different concentrations of APTDN and DPAN additives in 1 M HCl

Inhibitor	Conc., M	Activation parameters		
		E_a^*	ΔH^*	$-\Delta S^*$
		kJ/mol	kJ/mol	J/mol K
Free acid (1 M HCl)		42.2	21.2	111.4
APTDN	2×10^{-5}	36.3	14.6	168.5
	4×10^{-5}	34.1	14.3	174.8
	6×10^{-5}	32.0	13.4	185.4
	8×10^{-5}	30.7	12.7	193.7
	1×10^{-4}	28.9	12.8	195.5
DPAN	2×10^{-5}	26.4	14.8	166.0
	4×10^{-5}	24.9	14.1	172.7
	6×10^{-5}	23.5	12.5	186.0
	8×10^{-5}	22.7	11.7	193.4
	1×10^{-4}	22.0	11.8	196.8

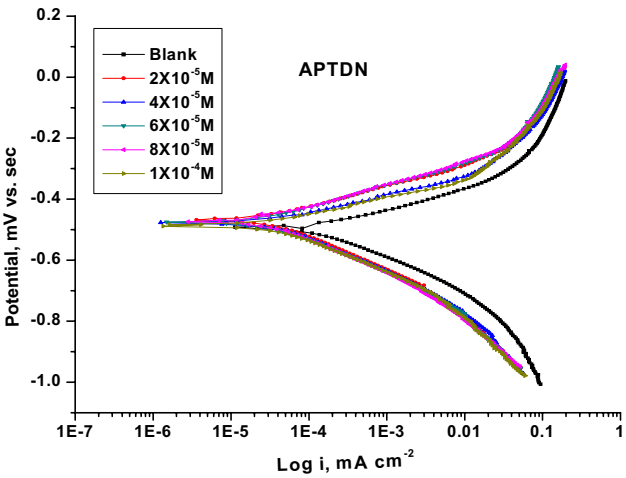

Fig. 6 PP plot for the corrosion of C-steel in 1 M HCl with and without different concentrations of APTDN at 25 °C

In order to calculate enthalpy and entropy of activation of ΔH^* and ΔS^*, the transition state equation was applied to calculate both parameters Eqs. (8, 9):

$$\text{C.R.} = \left[RT/\text{Nh}\right] \exp\left(\Delta S^*/R\right) \exp\left(-\Delta H^*/RT\right), \tag{8}$$

$$\text{Log C.R.} = \log\left[RT/\text{Nh}\right] + \left(\Delta S^*/R\right) - \left(\Delta H^*/RT\right) \tag{9}$$

[*h*] is the Planck's constant and [*N*] is the Avogadro's number. Plots log [C.R. /*T*] versus [1000/*T*] were shown in Fig. 5. Straight lines were obtained with a slope of $(-\Delta H^*/RT)$ and an intercept of $\log[R/\text{Nh}] + (\Delta S^*/R)$, and the values of ΔH^* and ΔS^* were computed. From the inspection data of Table 3, the positive values of ΔH^* point correspond to the endothermic nature of the activation process. Also it is clear that the with an increase in the activation entropy with the increase in the concentrations of the additives in positive direction, an increase in disordering happens from the reactant to the activated iron complex [36].

Table 4 Electrochemical parameter from PP for C-steel corrosion in 1 M HCl for APTDN and DPAN additives at 25 °C

Conc × 10^5, M		i_{corr} mA cm $^{-2}$	$-E_{corr}$, mV vs SCE	β_a mV/dec	$-\beta_c$, mV/dec	C.R mm/y	θ	$\%\eta$
Blank		150.0	493	71	122	98.17	–	–
APTDN	2	33.2	466	76	111	15.95	0.779	77.9
	4	32.7	477	62	106	15.72	0.782	78.2
	6	30.8	474	81	108	14.82	0.795	79.5
	8	28.9	472	80	109	13.91	0.807	80.7
	10	21.6	486	56	105	10.39	0.856	85.6
DPAN	2	38.9	453	84	110	16.16	0.741	74.1
	4	35.5	453	82	103	14.73	0.763	76.3
	6	32.9	421	64	123	13.67	0.780	78.1
	8	28.6	442	76	107	11.87	0.809	80.9
	10	27.0	442	74	103	11.23	0.820	82.0

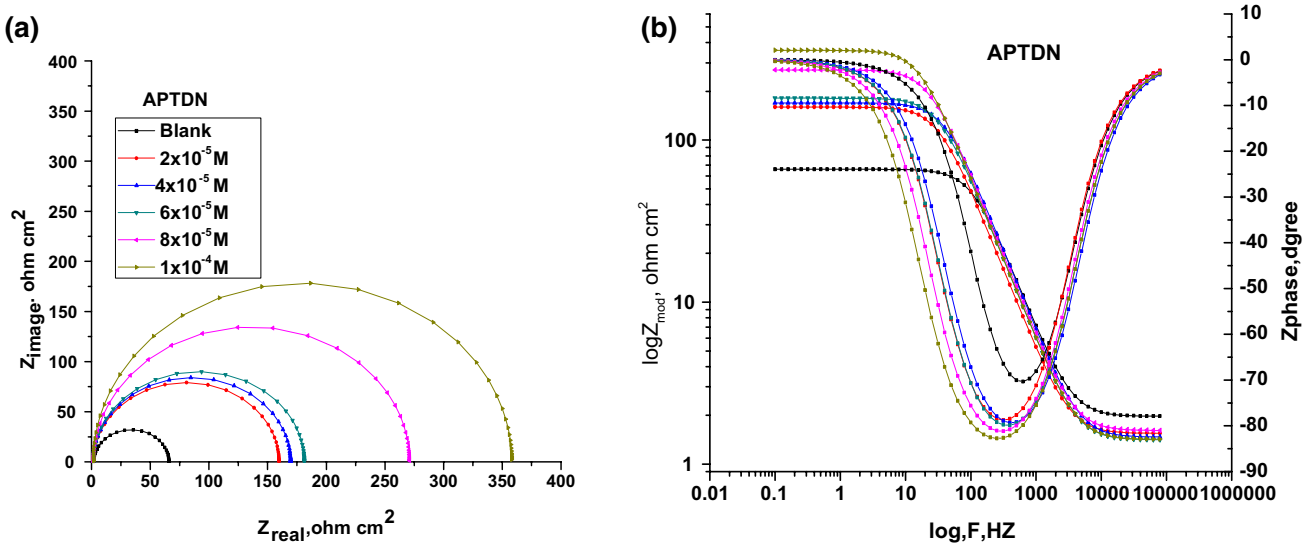

Fig. 7 The Nyquist (**a**) and Bode phase angle (**b**) plots for corrosion of C-steel in 1 M HCl in the absence and presence of various concentrations of APTDN at 25 °C

3.2 Potentiodynamic Polarization (PP) Measurements

The PP curves have been obtained for the C-steel electrode in acidic solution with and without different concentrations of APTDN at 25 °C, as shown in Fig. 6. That curves display the changes after adding APTDN additive which is used to classify individuals as cathodic, anodic, or mixed inhibitors [37]. The corrosion potential (E_{corr}), corrosion current density (i_{corr}), and anodic and cathodic Tafel slopes (β_a and β_c) have been calculated when the extrapolation of the linear portions of Tafel lines takes place [38]. Table 4 shows the reduction in i_{corr} and the increase in $\%\eta$ with increasing additive concentration. Also, it is observed that Tafel lines increase slightly with an increase in the concentration of APTDN and DPAN. This indicates that the two species

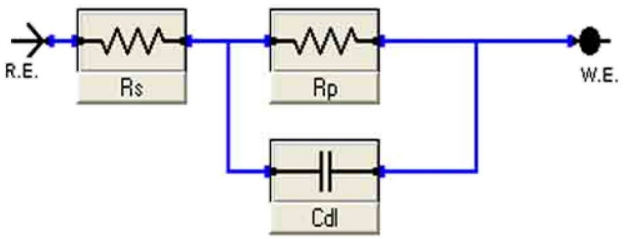

Fig. 8 Equivalent circuit model used to fit the impedance spectra

adsorb both the anodic and the cathodic sites [39]. The slight change in E_{corr} with range from 7 to 51 mV, that is less than 85 mV, [40] indicate that the two additives behaved as mixed-type inhibitors.

3.3 Electrochemical Impedance Spectroscopy

Figure 7 displays the EIS spectra in the form of Nyquist and Bode phase angle plots of C-steel working electrode in 1 M HCl with and without different concentrations of APTDN at 25 °C. The appearance of an individual capacitive loop signifying the behavior of a non-ideal capacitor of the steel surface / acid interface is obvious from Nyquist spectra [41]. Obviously, the diameter of capacitive loop is extended significantly by increased addition of the two tested compounds that gives the indication of the extent retardation of corrosion process [42]. Figure 8 presents a simple equivalent circuit which is used to analyze the EIS spectra through fitting the experimental results. This circuit includes charge transfer resistance (R_{ct}), solution resistance (R_s), and the constant phase element (CPE) which acts as ideal capacitor. Equation 10 determines the calculation of the capacitance double layer C_{dl} [43].

$$C_{dl} = {}^{1}/_{2}\pi f_{max} R_{ct} \tag{10}$$

where f_{max} represents the frequency at the maximum imaginary impedance in Nyquist diagram.

As shown in Table 5, the values of R_{ct} increased and C_{dl} decreased with an increase in the concentration of the two additives. The remarkable increase in the R_{ct} is due to the formation of adsorbed layer on C-steel surface which makes a barrier and delayed effectively by APTDN and DPAN molecules [44]. Also, the significant decrease in C_{dl} is related to the thickness of the protective layer which formed on the metal/electrolyte interface and also due to the replacement of the water molecules adsorbed on C-steel surface by the additive molecules [45]. As can be seen from Table 5, the $\%\eta$ of APTDN is high as 83% compared to 72.4% DPAN.

Table 5 Electrochemical kinetic parameters obtained from EIS technique for the corrosion of C- steel in 1 M HCl at various concentrations of APTDN and DPAN at 25 °C

[Inh]	Conc × 10^5, M	R_{ct}, Ω cm^2	$C_{dl} \times 10^{-5}$ μF/cm^2	Θ	$\%\eta$
1.0 M HCl	Blank	66.7	2.7600	–	–
APTDN	2	165.8	0.0137	0.600	60.0
	4	178.2	0.0115	0.626	62.6
	6	188.1	0.0106	0.646	64.6
	8	288.6	0.0042	0.769	76.9
	10	392.9	0.0023	0.830	83.0
DPAN	2	157.5	0.0202	0.576	57.6
	4	169.0	0.0171	0.605	60.5
	6	195.1	0.0136	0.658	65.8
	8	210.7	0.0116	0.683	68.3
	10	241.5	0.0094	0.724	72.4

This finding indicates that APTDN is highly adsorbed on the steel surface than DPAN which in agreement with the prior methods.

3.4 Electrochemical Frequency Modulation (EFM) Technique

The EFM is non-destructive and rapid technique to determine the corrosion current without prior information of Tafel slopes. The great strength in EFM is its causality factors which serve as an internal check on the validity of the EFM measurement [46]. Figure 9 displays the intermodulation spectrum of EFM of the target metal in 1 M HCl containing (2×10^{-5} M and 1×10^{-4} M) for APTDN and DPAN. Each spectrum signifies an observed current response versus frequency [47]. Table 6 indicates a variety of η EFM%, Tafel constants (β_a, β_c), and causality factors (CF-2 and CF-3) at different concentrations of the studied inhibitors. The corrosion current densities i_{corr} reduced by increasing the concentration of two derivatives as an effect to increase the adsorption power over the steel surface. Also, it is clear from Table 6 that the causality factor values CF-2 and CF-3 approached their theoretical values (2–3) indicating that the results of the corrosion parameters are verified and with high quality [48]. The greater $\%\eta$ values of APTDN related to DPAN which in agreement with prior measurements.

3.5 Quantum Chemical Parameters of Protonated Compounds

APTDN and DPAN compounds are optimized with Material Studio version 7.0 which illustrates the effect of the molecular structures and its relevant nature of electronic parameters on corrosion inhibition, the quantum parameters such as the energy values of the HOMO and LUMO orbitals and their energy gap ($\Delta E = E_{HOMO} - E_{LUMO}$), dipole moments, and molecular surface area of molecules [46], which are listed in Table 7. The HOMO orbit involves the ability of the molecule to donate electrons. On the contrary, The LUMO orbit involves the capability of the molecule to acquire electrons [49]. Basically, the electron affinity for any organic molecule is directly related to E_{HOMO} and E_{LUMO} values [50]. In accordance with the frontier molecular orbital theory, the formation of activated complex is attributed to the interaction between the (HOMO and LUMO) of the inhibitor and the d-vacant orbit of the metal [51]. Inspection of Table 7, E_{HOMO} of APTDN molecule is less high than the E_{HOMO} of DPAN molecule. It can be assumed that both molecules have an equal ability to offer electrons to d-vacant orbital of the steel. In the case of DPAN molecule, the electric

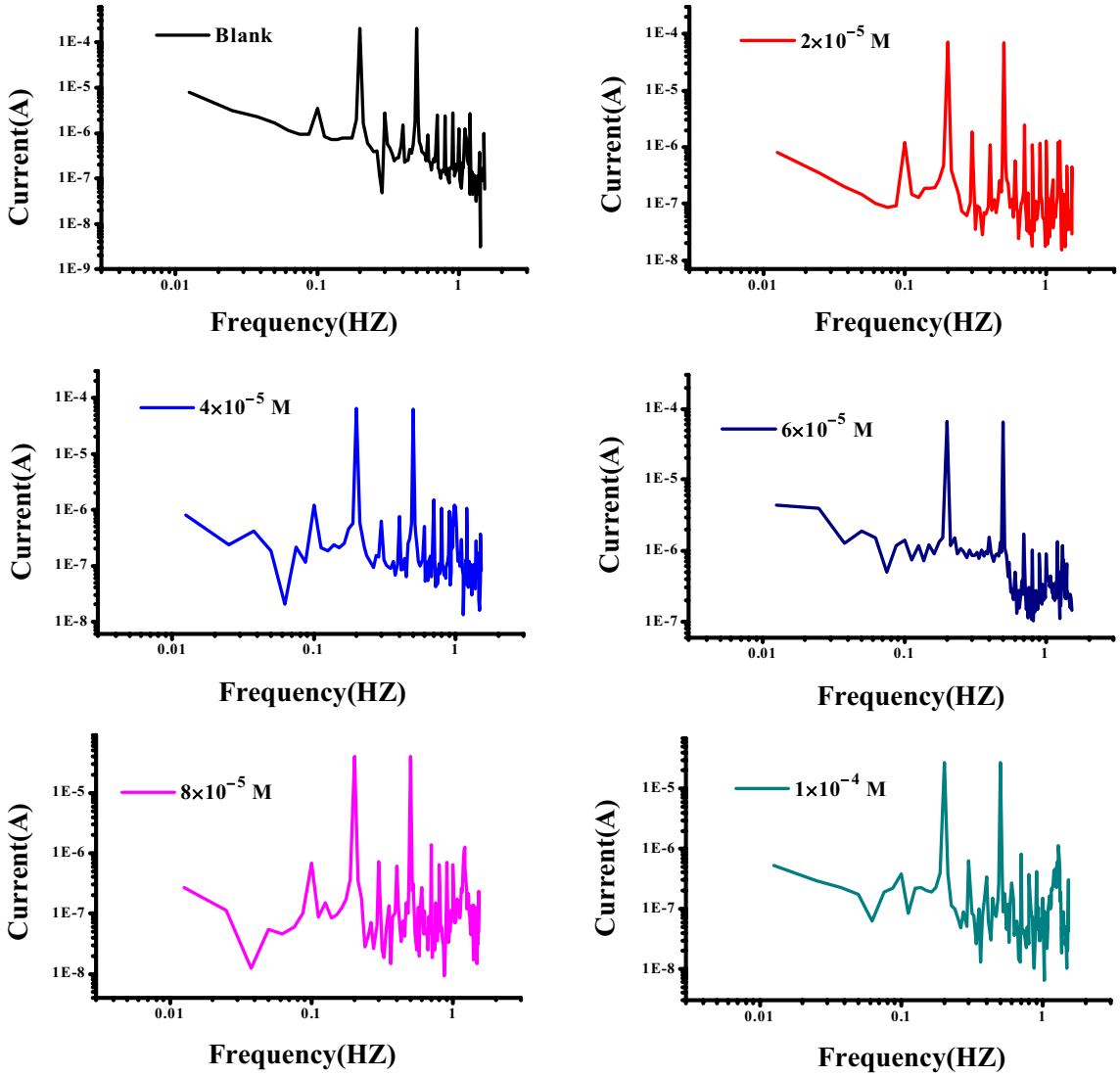

Fig. 9 EFM spectra of C-steel in 1 M HCl with and without various concentrations of APTDN at 25 °C

Table 6 Electrochemical parameters obtained from EFM technique for the corrosion of C-steel in 1 M HCl without and with APTDN and DPAN inhibitors at 25 °C

Comp	Conc × 10^5, M	i_{corr} μA/cm^2	β_a mV/dec	$-\beta_c$ mV/dec	CF-2	CF-3	Θ	$\%\eta$
1.0 M HCl Blank		299.2	93.72	101.3	1.89	2.96	–	–
APTDN	2	97.03	83.10	98.65	1.84	2.32	0.676	67.6
	4	88.64	85.74	93.92	1.14	2.46	0.704	70.4
	6	86.06	81.83	90.98	1.05	3.31	0.712	71.2
	8	49.34	75.59	86.01	1.67	3.24	0.835	83.5
	10	41.79	91.87	108.2	3.00	1.30	0.860	86.0
DPAN	2	109.5	102.6	109.3	1.88	2.26	0.634	63.4
	4	107.3	106.8	118.1	1.61	2.11	0.641	64.1
	6	87.41	104.1	120.7	1.85	2.66	0.708	70.8
	8	85.78	109.2	117.9	1.88	2.37	0.713	71.3
	10	83.36	94.5	126.3	1.96	2.32	0.721	72.1

Table 7 Quantum chemical parameters of the investigated compounds

	APTDN	DPAN
E_{HOMO}	− 4.377	− 4.763
E_{LUMO}	− 2.084	− 1.801
$\Delta E = (E_{LUMO} - E_{HOMO})$	2.293	2.962
Molecular surface area	274.69	259.171
Dipole moment	5.537	5.189

charge localized around pyridine ring and N atom, while in APTDN molecule its distributed on pyridine ring, S, and N atoms. As recognized, the electrons of carbon in pyridine ring are p-bonding type, while S and N atoms have non-bonding electron pairs, signifying that these heteroatoms are considered as the favorable sites for electrophile attack over the steel surface (Fig. 10). Also it is revealed from that table the energy gap of APTDN is proportionally small compared to the other inhibitor DPAN confirming that APTDN is an excellent corrosion inhibitor. Furthermore, the relevance between the molecular surface area and its efficiency is found; the more the molecular area value the more interaction area between the inhibitor and the metallic surface.

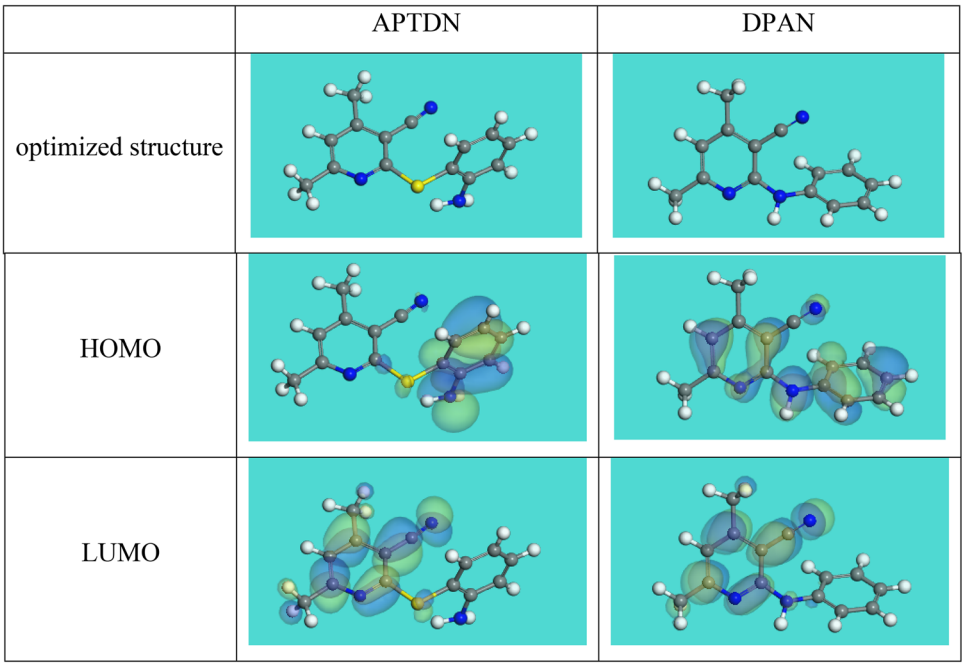

Fig. 10 The frontier molecular orbital for the examined inhibitors (HOMO and LUMO)

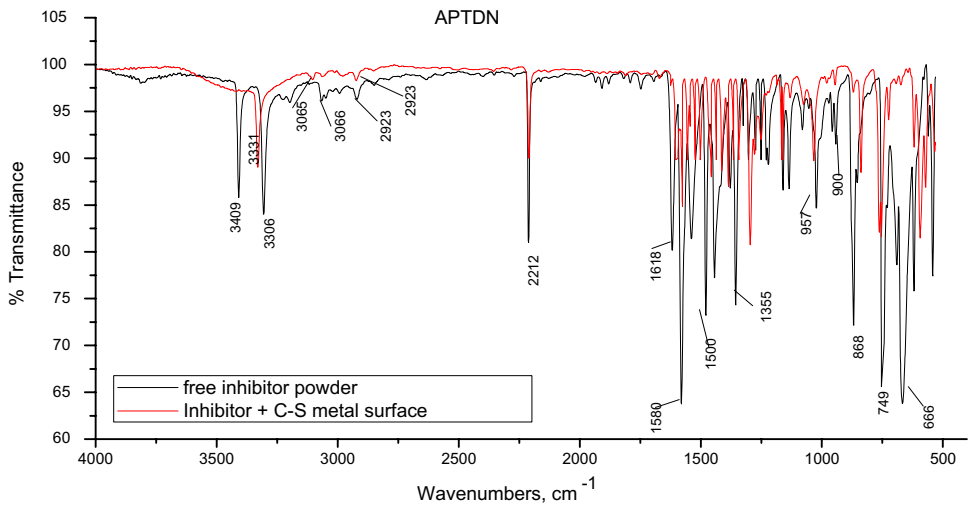

Fig.11 ATR-IR spectra of pure APTDN compound and C-steel metal surface in 1 M HCl + APTDN

Table 8 Characteristic peaks prior and after immersion in1 M HCl in the presence of APTDN for 24 h on C-steel surface at 25 ºC

Function group	Characteristic absorption (s) cm^{-1}	
	APTDN	
	Before	After
Stretching (NH–)	(3409,3306)	3331
Stretching (C–H) sp^2	3066	3065
Stretching (C–H) sp^3	2920	2923
Nitrile (C≡N)	2212	2211
Stretching (–C = N)	1618	1605
Bending (–NH–)	1580	1586
Stretching (–C = C)	1515	1527
Stretching (C–H) sp^3	1355	1349
Aromatic bending (C–H) sp^2	(957, 900)	(945,870)
Aromatic substituted	(868,749,666)	(838,750,594)

Table 9 AFM roughness data of the tested compounds (APTDN and DPAN) at 10×10^{-5} M for 24 h at 25 °C

Specimen	(R_a) nm	(R_q) nm
Series		
Blank	272.8	336.8
Pure	17.46	22.97
APTDN	49.8	64.2
DPAN	51.25	70.77

3.6 Surface Morphology

3.6.1 Attenuated Total Refraction Infrared (ATR-IR) Analysis

This method concerns for identifying the adsorbed functional groups of organic compounds on the C-steel surface. ATR-IR with a range 4000 to 400 cm^{-1} was performed. Figure 11 signifies the ATR-IR spectrum of APTDN inhibitor

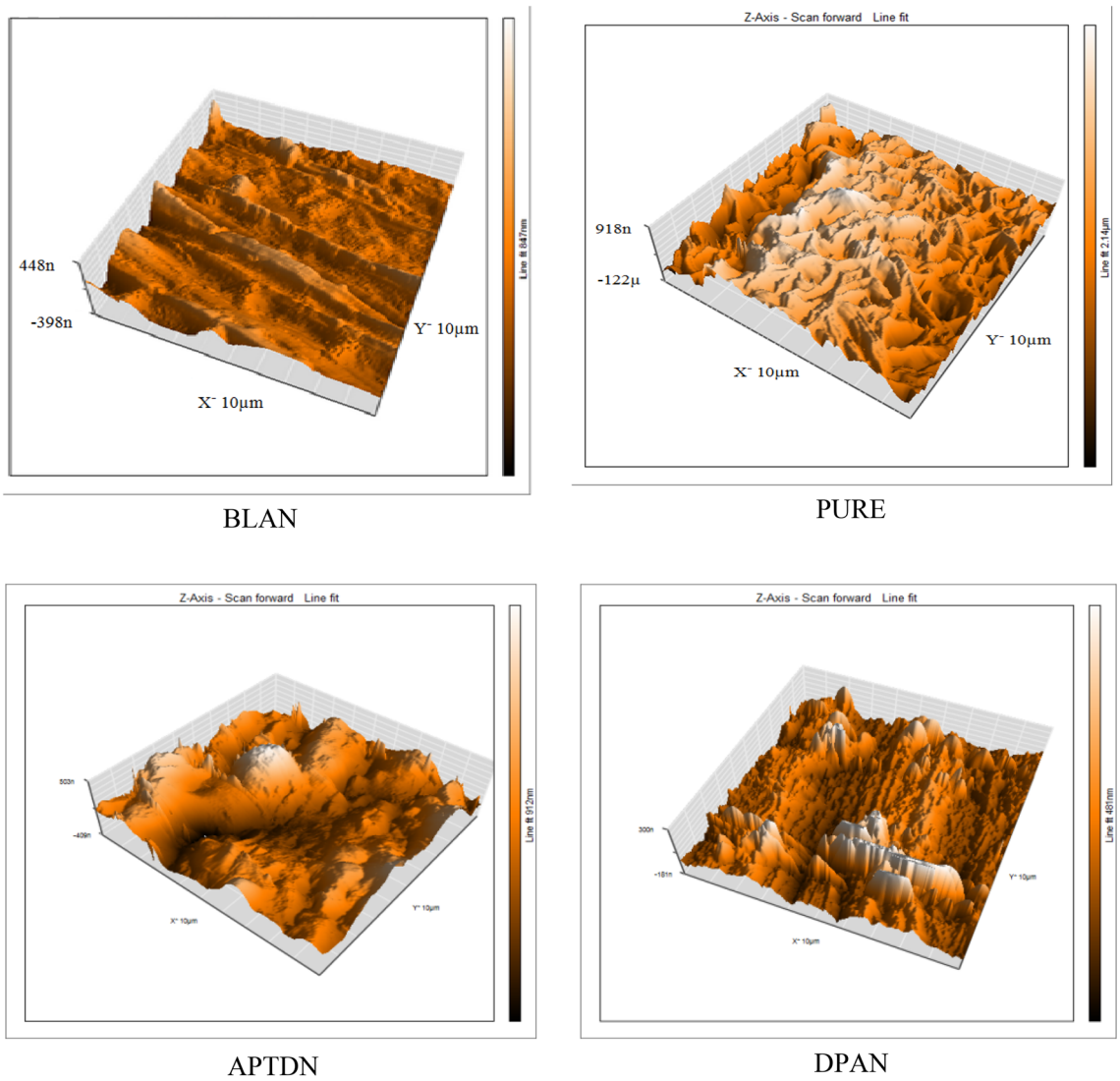

Fig. 12 AFM images for uninhibited and inhibited C-steel after immersion for 24 h in 1 M HCl for (APTDN, DPAN)

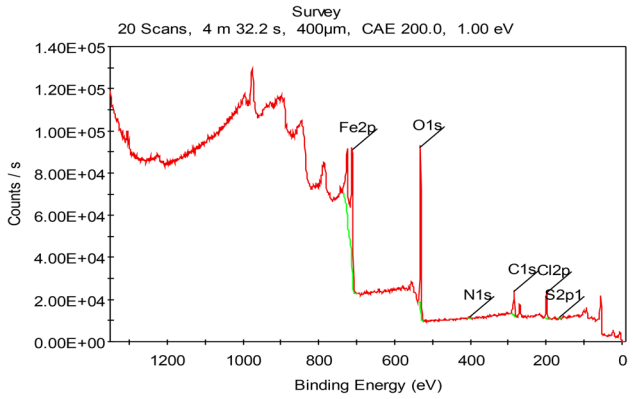

Fig. 13 The XPS survey spectrum results of APTDN adsorbed on the C-steel in 1 M HCl at 25 °C

and the construction of the adsorbed film over the steel surface after immersion for 24 h in 1 M HCl in the presence of APTDN. The characteristic peaks of active function groups for free organic compounds before (pure inhibitors) and the other peaks in the presence of these compounds after immersion for 24 h in the test solution on C-steel surface were discussed and scheduled in Table 8. The ATR-IR expresses the nature of the protecting film of the active function groups of APTDN on the C-steel surface in 1 M HCl after immersion for 24 h. From the clear peaks, there were small changes and some weak function groups frequencies disappeared such as two peaks of primary amine (NH–) in the pure compound, but converted to single peak of secondary amine surface (chemisorption) especially; also, others shifted due to the interaction and coordinate to the C-steel as shown in Table 8.

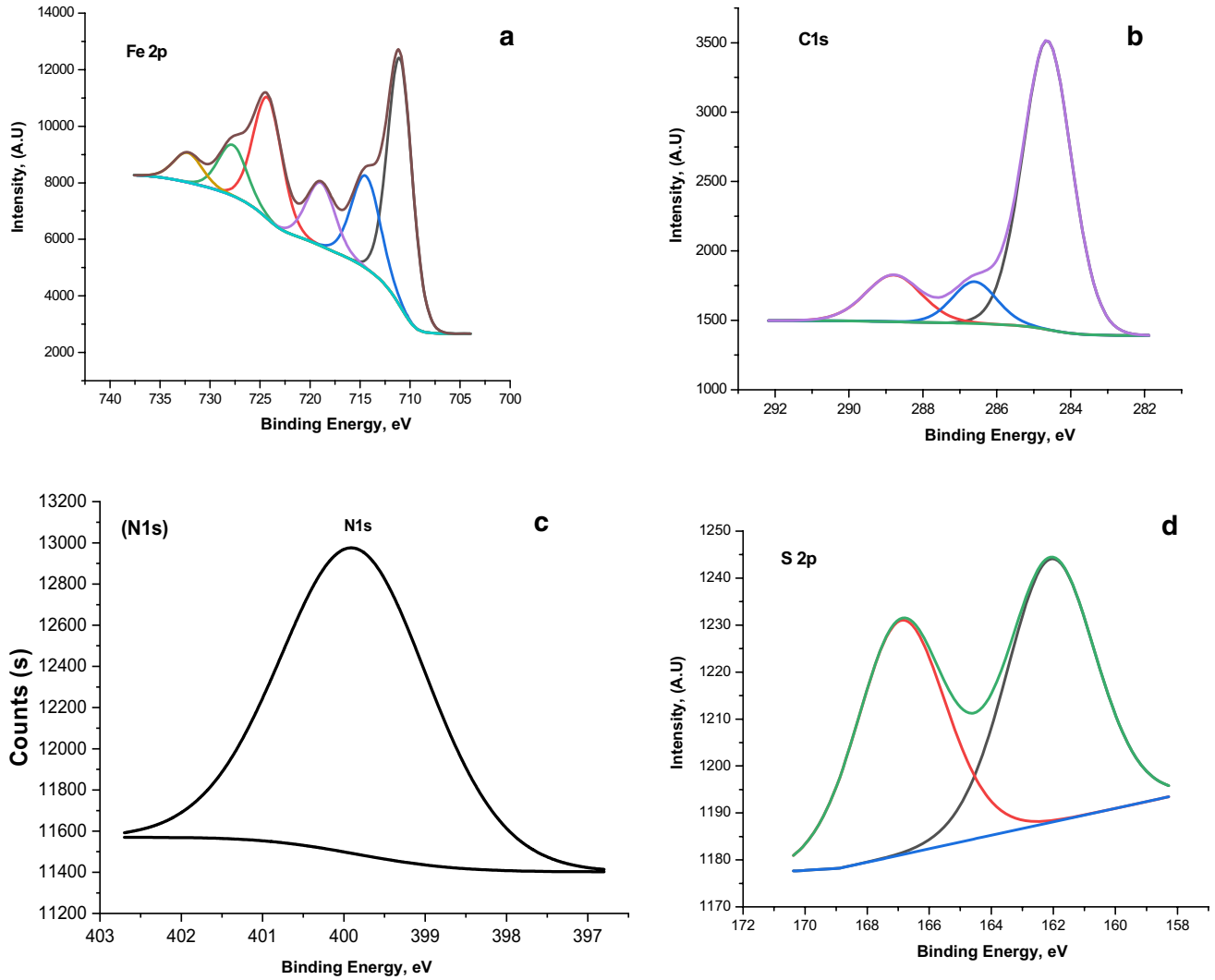

Fig. 14 High-resolution X-ray photoelectron deconvoluted profiles of **a** Fe 2p, **b** C 1 s, **c** N 1 s, and **d** S 2p for C-steel in 1 M HCl

The steel corrosion decreases after addition of APTDN inhibitor due to formation of the protective layer.

3.6.2 Atomic Force Microscopy (AFM) Analysis

AFM technique has been widely used in the analysis of the surface of metallic materials through the topographic maps that produce Nano level of metal /solution interface. Figure 12 displays the 3D images of the steel surface prior and after exposure to Hydrochloric acid solution for 24 h with and without addition of APTDN and DPAN. Table 9 presents the AFM parameters including Rq root mean square roughness and Ra average roughness. As expected, Rq and Ra values reduced at the entire adsorbed surface with APTDN and DPAN molecules that indicate a bright and smooth surface compared to the corroded surface in blank solution, but higher than the free sample.

3.6.3 X-Ray Photoelectron Spectroscopy Analysis

X-ray photoelectron spectroscopy (XPS) analysis was performed to confirm the adsorption of the investigated organic compounds on the steel surface and to determine the chemical nature of the inhibitors/carbon steel interface. The high-resolution XPS spectra obtained for carbon steel surface corroded in 0.1 M HCl in the presence of APTDN molecule as illustrated in Fig. 14. The Fe, O, C, Cl,N, and S elements with APTDN adsorption on the steel surface can be obviously seen. The spectrums of XPS of Cl 2p, N 1 s, C1s, O1s, S 2p, and Fe 2p are presented in Fig. 13, separately. Figure 14a presents the XPS spectrum of Fe 2p that shows six peaks. The high peak at lower binding energy (711.2 eV) corresponds to metallic iron [52]. The peak located at 714.6 eV is attributable to Fe 2p3/2, and the small peak at 719.40 eV corresponds to the satellite of Fe^{3+} [53]. In addition, the peaks at 724.3 eV and 727.9 eV can be attributed to Fe 2p1/2 due to the presence of iron in the form of Fe_3O_4, α-Fe_2O_3, and FeOOH [54]. The last peak at 732.4 eV is related to the oxidation of the steel surface. Figure 14b presents C 1 s spectra after APTDN molecule is adsorbed on the surface. It is found that more peaks are observed at 288.4 eV which is attributed to the sp2-hybridized carbon [55], in which comes from the inhibitor molecule.

Also, Fig. 14c shows XPS spectrum of N 1 s with a single peak at 399.9 eV, this peak could be attributed to the neutral imine (–N=) and amine (–N–H) nitrogen atoms as previously reported [56, 57]. Finally, XPS spectrum of S 2p is showed in Fig. 14d which presented two spin–orbit-split doublets for S 2p3/2 and S 2p1/2, with binding energies at 162.1 and 166.8 eV, which correspond to the sulfide species and the C–S bond, respectively. According to the XPS results, we can confirm the adsorption of the investigated inhibitors on the C-steel surface in HCl solution.

References

1. Raja PB, Ismail M, Ghoreishiamiri S, Mirza J, Ismail MC, Kakooei S, Rahim AA (2016) Reviews on corrosion inhibitors: a short view. Chem Eng Commun 203:1145–1156
2. ISO 8044:2015. Corrosion of metals and alloys—basic terms and definitions. 8044:2015–2017
3. Samide A, Iacobescu GE, Tutunaru B, Grecu R, Tigae C, Spînu C (2017) Inhibitory properties of neomycin thin film formed on carbon steel in sulfuric acid solution: electrochemical and AFM investigation. Coatings 7(181):1–12
4. Verma MAC, Quraishi MA, Ebenso EE (2018) Microwave and ultrasound irradiations for the synthesis of environmentally sustainable corrosion inhibitors: an overview. Sust Chem Pharm 10:134–147
5. Gupta M, Mishra J, Pitre KS (2013) Corrosion and ınhibition effects of mild steel in hydrochloric acid solutions containing organo phosphonic acid. Int J Corros 1:1–5
6. Shaban SM, Saied A, Tawfik SM, Abd-Elaal A, Aiad I (2013) Corrosion inhibition and biocidal effect of some cationic surfactants based on Schiff base. J Ind Eng Chem 19:2004–2009
7. Meng Y, NingW XuB, YangW ZK, Chen Y (2017) Inhibition of mild steel corrosion in hydrochloric acid using two novel pyridine Schiff base derivatives: a comparative study of experimental and theoretical results. RSC Adv 7(68):43014–43029
8. Krim O, Elidrissi A, Hammouti B, Ouslim A, Benkaddour M (2009) Synthesis, characterization, and comparative study of pyridine derivatives as corrosion inhibitors of mild steel in HCl medium. Chem Eng Commun 196(12):1536–1546
9. Finšgar M, Jackson J (2014) Application of corrosion inhibitors for steels in acidic me-dia for the oil and gas industry: a review. Corros Sci 86:17–41
10. Al-Sarawy AA, Diab MA, El-Desoky AM, El-Bindary RA (2013) Adsorption and inhibitive properties for corrosion of carbon steel in hydrochloric acid solution by some nicotinonitrile derivatives. Int J Sci Eng Res 4:690–698
11. Priyanka Singh M, Makowska-Janusik PS, Quraishi MA (2016) Nicotinonitrile as green corrosion inhibitors for mild steel in hydrochloric acid: electrochemical, computational and surface morphological studies. J Mol Liq 220:71–81
12. Baddar FG, Al-Hajjar FH, El-Rayyes NR (1976) Acetylenic ketones. I. Reaction of aroylphenylacetylenes with compounds containing an active methylene group. J Chem 13:195–203
13. Mariella RP, Leech JL (1949) The synthesis of some isomeric dimethyl-hydroxymethylpyridines. 3,4-Didesoxypyridoxin. J Am Chem Soc 71:331–333
14. Kalme ZA, Roloff B, Pelcher YE, Popelis YY, Khagen F, Dubur GY (1992) Nucleophilic substitution reactions in 2-chloropyridines and 2,5-dioxo-1,2,5,7-tetrahydro-1H-furo[3,4-b] pyridines. Chem Heterocyc Compd 28(1411):1031–1035
15. Abdel-Latif E, Metwally MA (2007) Waste-free solid-state organic syntheses: solvent-free alkylation, heterocyclization, and Azo-coupling reactions. Monatshefte Chemie 138:771–776
16. ASTM International. ASTM G31-72 (1999) Standard practice for laboratory immersion corrosion testing of metals. West Conshohocken: ASTM International
17. Fernandez-Solis CD, Vimalanandan A, Altin A, Mondragon-Ochoa JS, Keil KK, Erbe A (2016) Fundamentals of electrochemistry, corrosion and corrosion protection: In Lang PR, Liu Y (eds) Soft matter at aqueous interfaces. Springer, Basel
18. Matad PB, Mokshanatha PB, Hebbar N, Venkatesha VT, Tandon HC (2014) Ketosulfone drug as a green corrosion inhibitor for mild steel in acidic medium. Ind Eng Chem Res 53:8436–8444

19. Khaled KF (2009) Monte Carlo simulations of corrosion inhibition of mild steel in 0.5 M sulphuric acid by some green corrosion inhibitors. J Solid State Electrochem 13:1743–1756
20. Ahamad I, Gupta C, Prasad R, Quraishi MA (2010) An experimental and theoretical investigation of adsorption characteristics of a Schiff a base compound as corrosion inhibitor at mild steel/hydrochloric acid interface. J Appl Electrochem 40:2171–2183
21. Shukla SK, Ebenso EE (2011) Corrosion inhibition, adsorption behavior and thermodynamic properties of streptomycin on mild steel in hydrochloric acid medium. Int J Electrochem Sci 6:3277–3291
22. Moussa MNH, El-Far AA, El-Shafei AA (2007) The use of water soluble hydrazones as inhibitors for the corrosion of c-steel in acidic medium. Mater Chem Phys 105:105–113
23. Singh DK, Kumar S, Udayabhanu G, John RP (2016) 4(N, N-dimethylamino) benzaldehyde nicotinic hydrazone as corrosion inhibitor for mild steel in 1 M HCl solution: an experimental and theoretical study. J Mol Liq 216:738–746
24. Ozcan M, Solmaz R, Kardas G, Dehri I (2008) Adsorption properties of barbiturates as green corrosion inhibitors on mild steel in phosphoric acid. Colloids Surf A 325:57–63
25. Abiola OK, Oforka NC (2004) Adsorption of (4-amino-methyl-5-pyrimidinyl methylthio) acetic acid on mild steel from hydrochloric acid solution (HCl)-Part 1. Mater Chem Phys 83:315–322
26. Li X, Deng S, Fu H (2011) Triazolyl blue tetrazolium bromide as a novel corrosion inhibitor for steel in HCl and H_2SO_4 solutions. Corros Sci 53:302–309
27. Deng S, Li X, Fu H (2011) Two pyrazine derivatives as inhibitors of the cold rolled steel corrosion in hydrochloric acid solution. Corros Sci 53:822–828
28. Ateya BG, El-Anadouli BE, El-Nizamy FM (1984) The adsorption of thiourea on mild steel. Corros Sci 24:509–515
29. Bhat JI, Alva VDP (2011) Inhibition effect of nevirapine an antiretroviral on the corrosion of mild steel under acidic condition. J Korean Chem Soc 55:835–841
30. Oguzie EE, Okolue BN, Ebenso EE (2004) Evaluation of the inhibitory effect of methylene blue dye on the corrosion of Al in hydrochloric acid. Mater Chem Phys 87:394–401
31. Marcus P (2002) Corrosion mechanisms in theory and practice, 2nd edn. Marcel Dekker Inc., New York
32. Obot IB, Obi-Egbedi NO, Umoren SA (2009) Antifungal drugs as corrosion inhibitors for Al in 0.1 M HCl. Corros Sci 51:1868–1875
33. Oguzie EE, Njoku VO, Enenebeaku CK, Akalezi CO, Obi C (2008) Effect of hexamethylpararosaniline chloride (crystal violet) on mild steel corrosion in acidic media. Corros Sci 50:3480–3486
34. Prabhu D, Rao P (2013) Coriandrum sativum L.—a novel green inhibitor for the corrosion inhibition of Al in 1.0 M phosphoric acid solution. Chem Eng 1:676–683
35. Ramazan S (2014) Investigation of adsorption and corrosion inhibition of mild steel in hydrochloric acid solution by 5-(4-dimethylaminobenzylidene) rhodanine. Corros Sci 79:169–176
36. Xu B, Yang WZ, Liu Y, Yin XS, Gong WN, Chen YZ (2014) Experimental and theoretical evaluation of two pyridine carboxaldehydethiosemicarbazone compounds as corrosion inhibitors for mild steel in hydrochloric acid solution. Corros Sci 78:260–268
37. Bahrami MJ, Hosseini SMA, Pilvar P (2010) Experimental and theoretical investigation of organic compounds as inhibitors for mild steel corrosion in sulfuric acid medium. Corros Sci 52:2793–2803
38. Raja PB, Qureshi AK, Abdul Rahim A, Osman H, Wang KA (2013) Neolamarckiacadamba alkaloids as eco-friendly corrosion inhibitors for mild steel in 1 M HCl media. Corros Sci 69:292–301
39. Fiori-Bimbi MV, Alvarez PE, Vaca H, Gervasi CA, Reza I, Saleemi AR et al (2015) Corrosion inhibition of mild steel in HCL solution by pectin. Corros Sci 92:192–199
40. Markhali BP, Naderi R, Mahdavian M, Sayebani M, Arman SY (2013) electrochemical impedance spectroscopy and electrochemical noise measurements as tools to evaluate corrosion inhibition of azole compounds on stainless steel in acidic media. Corros Sci 75:269–279
41. Tang Y, Zhang F, Huc S, Cao Z, Wu Z, Jing W (2013) Novel benzimidazole derivatives as corrosion inhibitors of mild steel in the acidic media. Part I: Gravimetric, electrochemical. SEM and XPS studies Corros Sci 74:271–282
42. Bosch RW, Bogaerts WF (1996) Instantaneous corrosion rate measurement with small-amplitude potential intermodulation techniques. Corrosion 52:204–212
43. El-Askalany AH, Mostafa SI, Shalabi K, Eid AM, Shaaban S (2016) Novel tetrazole-based symmetrical diselenides as corrosion inhibitors for N80 carbon steel in 1 M HCl solutions: experimental and theoretical studies. J Mol Liq 223:497–508
44. Noor EA, Al-Moubaraki AH (2008) Thermodynamic study of metal corrosion and inhibitor adsorption processes in mild steel/1-methyl-4[4'(-X)-styryl pyridinium iodides/hydrochloric acid systems. Mater Chem Phys 110:145–154
45. Amin MA, EI-Rehim SSA, El-Sherbini EEF, Hazzazi OA, Abbas MN (2009) Polyacrylic acid as a corrosion inhibitor for Al in weakly alkaline solutions. Part I: weight loss, polarization, impedance EFM and EDX studies. Corros Sci 51:658–667
46. Amin MA, Abd El Rehim SS, Abdel-Fatah HTM (2009) Electrochemical frequency modulation and inductively coupled plasma atomic emission spectroscopy methods for monitoring corrosion rates and inhibition of low alloy steel corrosion in HCl solutions and a test for validity of the tafel extrapolation method. Corros Sci 51:882–889
47. Abd El-Raouf M, Khamis EA, Abou Kana MTH, Negm NA (2018) Electrochemical and quantum chemical evaluation of new bis(coumarins) derivatives as corrosion inhibitors for carbon steel corrosion in 0.5 M H_2SO_4. J Mol Liq 255:341–353
48. Mo S, Luo HQ, Li NB (2017) Study on the influences of two thiazole flavor ingredients on Cu corrosion caused by chloride ion. J Colloid Interface Sci 505:929–939
49. Kosari A (2014) Electrochemical and quantum chemical assessment of two organic compounds from pyridine derivatives as corrosion inhibitors for mild steel in HCl solution under stagnant condition and hydrodynamic flow. Corros Sci 78:138–150
50. Finsgar M, Lesar A, Kokalj A, Milosev I (2008) A comparative electrochemical and quantum chemical calculation study of BTAH and BTAOH as copper corrosion inhibitors in near neutral chloride solution. Electrochim Acta 53:8287–8297
51. Boumhara K, Tabyaoui M, Jama C, Bentiss F (2015) Artemisia Mesatlantica essential oil as green inhibitor for carbon steel corrosion in 1 M HCl solution: electrochemical and XPS investigations. J Ind Eng Chem 29:146–155
52. El Hamdani N, Fdil R, Tourabi M, Jama C, Bentiss F (2015) Alkaloids extract of Retama monosperma (L.) Boiss. Seeds used as novel eco-friendly inhibitor for carbon steel corrosion in 1 M HCl solution. Appl Surf Sci 357:1294–1305
53. Gao X, Liu S, Lu H, Gao F, Ma H (2015) Corrosion inhibition of iron in acidic solutions by monoalkyl phosphate esters with different chain lengths. Ind Eng Chem Res 54:1941–1952
54. Wang X, Yang W, Li F, Xue Y, Liu R, Hao Y (2013) In situ microwave-assisted synthesis of porous N-TiO_2/g-C_3N_4 heterojunctions with enhanced visible-light photocatalytic properties. Ind Eng Chem Res 52:17140–17150
55. Thomas A, Fischer A, Goettmann F, Antonietti M, Schloegl MJ, Carlsson R (2008) J.-M. Graphitic carbon nitride materials: variation of structure and morphology and their use as metal-free catalysts. J Mater Chem 18:4893–4908
56. Gu T, Chen Z, Jiang X, Zhou L, Liao Y, Duan M et al (2015) Synthesis and inhibition of N-alkyl-2-(4-hydroxybut-2-ynyl)

pyridinium bromide for mild steel in acid solution: Box-Behnken design optimization and mechanism probe. Corros Sci 90:118–132
57. Meneguzzi A, Ferreira CA, Pham MC, Delamar M, Lacaze PC (1999) Electrochemical synthesis and characterization of poly(5-amino-1-naphthol) on mild steel electrodes for corrosion protection. Electrochim Acta 44:2149–2156